STUDY OF ABSORPTION IN THE INNER EAR AND THE VESTIBULO-COCHLEAR NERVE FROM MOBILE PHONE EXPOSURE

R. Kopecký*, H. Nellström** and M. Persson*

* Dept. of Electromagnetics, Chalmers University of Technology, Göteborg, Sweden
** Diagnostic Radiology and Neuroradiology, Medorad AB, Kungsbacka, Sweden

elfrk@chalmers.se

Abstract: The aim of this study is to model electromagnetic field from a mobile phone exposure in the region of the inner ear and the internal acoustic canal. The Finite Difference Time Domain method and subgridding technique are used to calculate Specific Absorption Rate distribution in a human head model. The head model is improved in the region of the inner ear by insertion of more detailed inner ear model created from CT slices.

Introduction

If radio-frequency exposure from mobile phone use increases the risk of cancer, acoustic neuroma is of potential concern. A recent study [1] suggests an increased risk of acoustic neuroma associated with extensive long term mobile phone usage.

An acoustic neuroma, also termed as a neurinomma or vestibular schwannoma, is a benign or non-cancerous growth that arises from the vestibulo-cochlear nerve. This nerve is in reality 2 separate nerves - the vestibular nerve and the cochlear nerve. The vestibular nerve is responsible for balance while the cochlear nerve is responsible for hearing. The vestibular nerve has 2 parts- the superior vestibular nerve and the inferior vestibular nerve. These nerves lie adjacent to each other as they pass through a bony canal, the internal acoustic canal, from the inner ear to the brain system.

This paper is concerned with the computer modelling of electromagnetic field from a mobile phone in the region of the inner ear and in the region of the internal acoustic canal. Of special interest is the question of how detailed models need to be to give reliable results in the specific absorbed power. The numerical method used is the Finite Difference Time Domain (FDTD) method [2]. In order to model the Specific Absorption Rate (SAR) distribution in the region of the inner ear at sufficient resolution a subgridding technique is used.

Materials and Methods

The head model, Figure 1, is a tissue-classified version of the Visible Human Project [3] male data set based on anatomical slices developed at Brooks Air Force Base Laboratories [4]. The head model has a geometrical resolution of 1 mm and contains 24 biological tissues. The dielectric properties of the biological tissues are those reported by Gabriel [5].

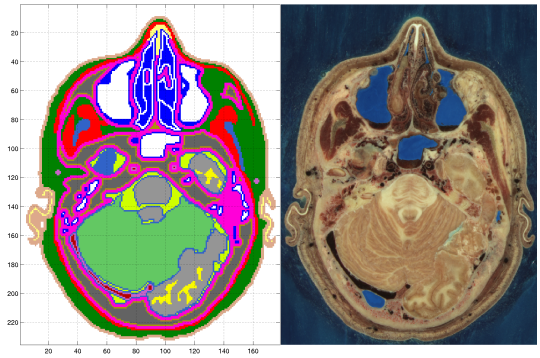

Figure 1: Computer head model and original anatomical slice from Visible Human Project.

Because of the geometrical resolution the inner ear tissues are not included in the head model. The reason is that 1 mm geometrical resolution of the model is too coarse in order to include tiny structure of the inner ear. It was therefore necessary to create a new inner ear model and insert it into the head model with locally increased resolution.

The inner ear model was obtained from a set of 53 horizontal CT slices of an anonymous patient, Figure 2(a-c). Resolution of CT slices was 0.1562 mm (160 mm/1024 pixels) and distance between the slices was 0.1 mm. From these CT slices the inner ear model was reconstructed using edge detection image filtering, Figure 2(d) and window filtering, Figure 2(e). Edge detection using Canny method was used together with window filtering of range between 1 and 120 Hounsfield Units. CT images were gray scaled images with gray levels between 0 and 255 Hounsfield Units. Manual corrections were necessary in order to smooth the model and hence decrease the staircase errors of the model, Figure 2(f). Finally the inner ear model was inserted into the head model to the correct position, Figure 3. The inner ear model consists of cochlea, vestibule, and semicircular canals, Figure 4.

The FDTD code used for the SAR calculation uses the Yee algorithm [6] based on the composition of electric and magnetic field components shown in Figure 6. This formulation differs from the original Yee formula-

ISSN: 1727-1983

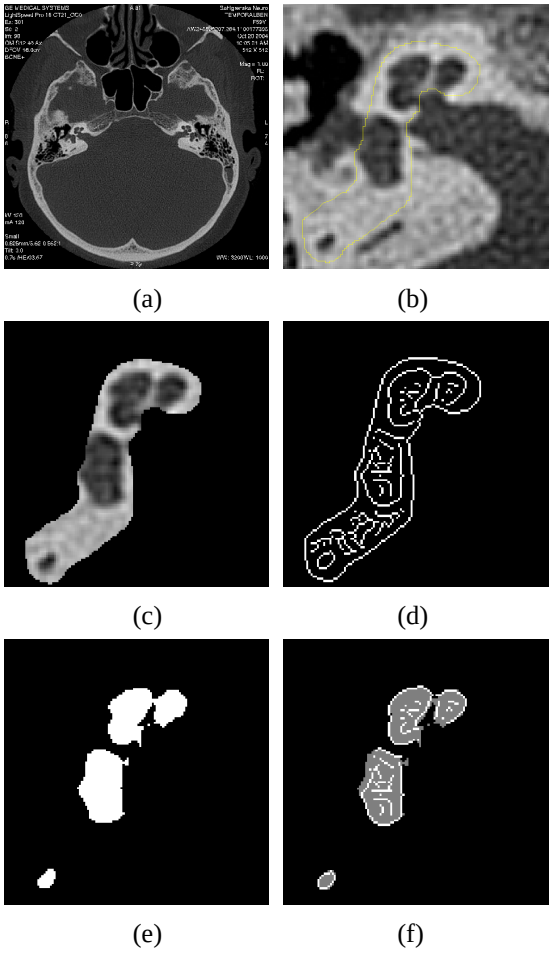

(a) (b) (c) (d) (e) (f)

Figure 2: (a) A CT image of a horizontal cut through a human head. (b),(c) The detail of the left inner ear region. (d) Edge filtering using the Canny method. (e) Simple window filtering (from 1 to 120 HU). (f) The resulted model before manual corrections.

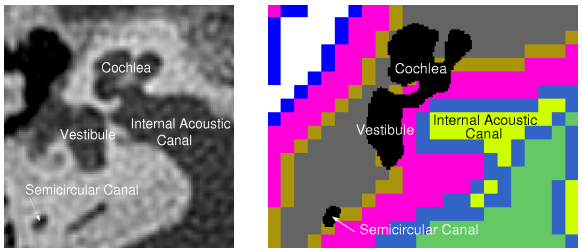

(a) (b)

Figure 3: Insertion of the inner ear model into the head. (a) The inner ear region in a CT picture. (b) The inner ear model inserted into the computer head model.

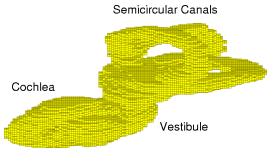

Figure 4: 3D view of the inner ear model.

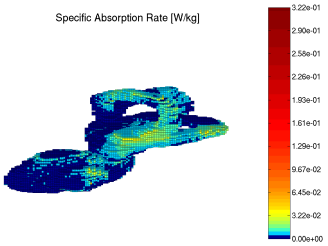

Figure 5: Specific Absorption Rate distribution on the surface of the inner ear model.

tion in a way that makes it suitable for modelling in biological tissues, when a subgridding technique introduced by Chevalier [7] is used.

This subgridding technique is suitable there, where non-magnetic materials traverse the subgrid. The technique allows to use a subgrid cell ratio of an odd number. Subgrid cell ratio is the ratio between the main grid cell size and the subgrid cell size.

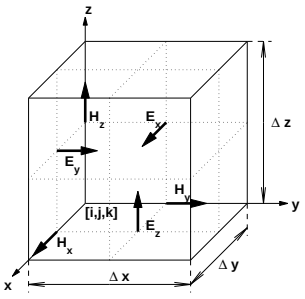

Figure 6: The Yee cell at location i, j, k with the magnetic vectors on edges and the electric vectors centred on sides.

The geometrical resolution of the inner ear model is 0.1562 mm in horizontal directions and 0.1 mm in vertical direction. The model was resampled in order to achieve resolution 0.111 =1/9 mm in all directions, because then the ratio between the resolution of the head and the resolution of the inner ear is equal to 9 and the subgridding with this cell ratio can be used.

On the other hand, the subgrid cell ratio of 9 is quite large, there would be a huge jump between the main grid

ISSN: 1727-1983

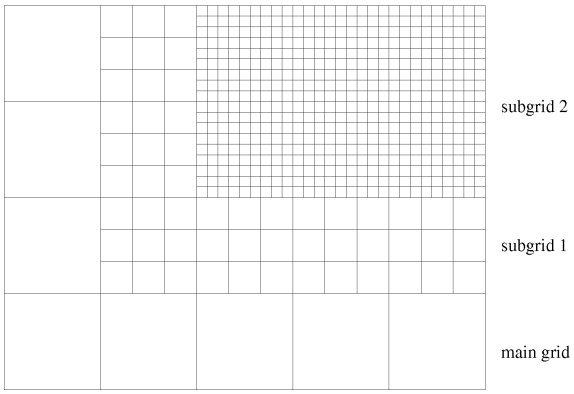

Figure 7: Nesting of two subgrids of cell ratio of 3 results in the subgrid cell ratio of 9.

cell size and the subgrid cell size, if only one subgrid was used. It is therefore more convenient to use two nested subgrids with the cell ratios equal to 3 (Figure 7) rather then one subgrid with the cell ratio of 9. Then the total cell ratio is the same, but a smother transition of the field through the subgrids is achieved.

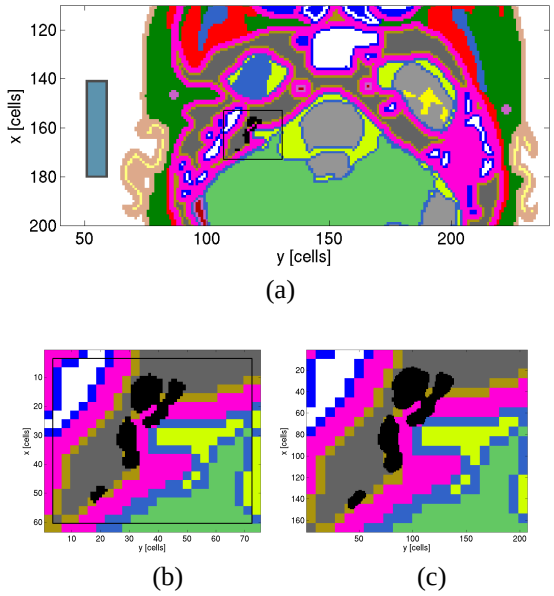

Figure 8: (a) The main grid. The cell size is 1 mm. (b) The subgrid #1 with the cell size of 0.333 mm. (c) The subgrid #2, where the size of cells is 0.111 mm.

Figure 8 shows a realization of nesting of two subgrids into the main grid. In Figure 8(a) is illustrated a cross-section through the head in the main grid. The boundary between the main grid and the subgrid #1 is depicted as the black rectangle. Figure 8(b) illustrates the subgrid #1. The boundary between the subgrid #1 and the subgrid #2 is drawn as the black rectangle. Figure 8(c) shows the subgrid #2. Only here the inner ear model has a geometrical resolution of 0.111 mm. In the subgrid #1 the geometrical resolution of the inner ear is resampled to 0.333 mm and in the main grid to 1 mm.

The head model was exposed to a mobile phone radiation in the GSM 1800 MHz band at an average output power of 0.125 W and a transmitting frequency of 1750 MHz. The mobile phone was modelled using a generic model consisting of a $\lambda/4$ monopole antenna of 0.4 mm diameter centred on a metallic box of size $10 \times 40 \times 80$ mm covered by a 1-mm plastic isolation (ε_r=2.46, σ=4.47·10^{-4} S/m). The phone was placed in vertical position touching the head.

Results

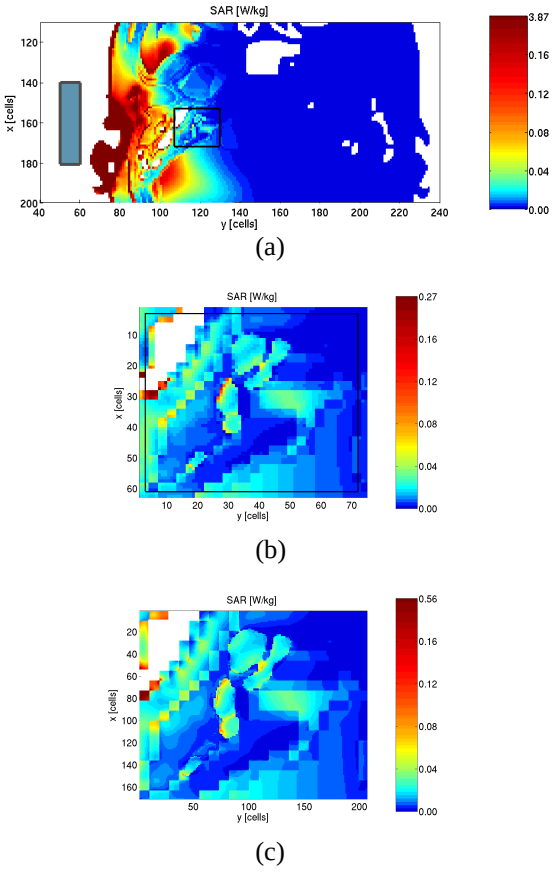

Figure 9: Specific Absorption Rate distribution in a horizontal cross-section through the head: (a) SAR in the main grid. (b) SAR in the subgrid #1. (c) SAR in the subgrid #2.

Results from simulations, SAR in the inner ear (IE) and the internal acoustic canal (IAC) are listed in Tables 1-2 and Tables 3-4, respectively. The SAR is averaged over the tissue volume of the organs. The volume of the IE is 92.49 mm^3, the volume of the IAC is 67.17 mm^3 and the weight of the IE and the IAC is in order of tens of milligrammes. Therefore the SAR is averaged over the volume of organs rather than over 10 g specified by ICNIRP [8].

ISSN: 1727-1983

In Table 1 the inner ear model has different resolution through the grids. With decreasing resolution the volume of the inner ear model increases from 92.49 mm^3 to 102 mm^3 and the volume averaged SAR increases from $3.19{\cdot}10^{-2}$ to $3.28{\cdot}10^{-2}$ W/kg. The increase is not significant showing that insertion of a fine model of the inner ear into the coarse model of the head does not improve result in term of tissue volume averaged SAR. In Figure 9 the volume averaged SAR is plotted in the same horizontal slice as illustrated in Figure 8.

It is interesting to observe what will happen if the geometrical resolution of the IE region in the head model is improved together with the IE model. The improvement of the region consists in smoothing of the staircase approximation. Boundaries between biological tissues were detected and smoothed using an interpolation. The smoothed model is shown in Figure 10(a).

In Table 2 the results are listed for IE in the smoothed IE region. By smoothing the geometry of the IE region and decreasing staircase approximation, the volume averaged SAR is lower compared to the case in Table 1 about approximately 10%.

In Table 3 the IAC has the same geometrical resolution through the grids. The IAC is therefore the same in all grids and the volume would be the same if the IE model did not overlap a part of the IAC. However the SAR in the IAC decreased from $2.08{\cdot}10^{-2}$ W/kg in the subgrid #2 to $2.06{\cdot}10^{-2}$ W/kg in the main grid. This decrease is also not significant, it is caused only by changing of the numerical resolution and consequently by staircase approximation errors.

After smoothing the IE region, the volume averaged SAR in the IAC increased by 5%. This is in contrast to the case of the inner ear. The results are listed in Table 4.

Table 1: Volume averaged SAR in the inner ear.

grid:	SAR[W/kg]	volume[mm^3]
subgrid #2	$3.19{\cdot}10^{-2}$	92.49
subgrid #1	$3.30{\cdot}10^{-2}$	94.59
main grid	$3.28{\cdot}10^{-2}$	102

Table 2: Volume averaged SAR in the inner ear. The inner ear region in the head is improved by smoothing the contours of the tissues.

grid:	SAR[W/kg]	volume[mm^3]
subgrid #2	$2.91{\cdot}10^{-2}$	92.49
subgrid #1	$3.08{\cdot}10^{-2}$	94.59
main grid	$3.28{\cdot}10^{-2}$	102

Table 3: Volume averaged SAR in the internal acoustic canal.

grid:	SAR[W/kg]	volume[mm^3]
subgrid #2	$2.08{\cdot}10^{-2}$	64.47
subgrid #1	$2.08{\cdot}10^{-2}$	65.29
main grid	$2.06{\cdot}10^{-2}$	69

Table 4: Volume averaged SAR in the internal acoustic canal. The inner ear region in the head is improved by smoothing the contours of the tissues.

grid:	SAR[W/kg]	volume[mm^3]
subgrid #2	$2.19{\cdot}10^{-2}$	67.17
subgrid #1	$2.28{\cdot}10^{-2}$	64.29
main grid	$2.59{\cdot}10^{-2}$	71

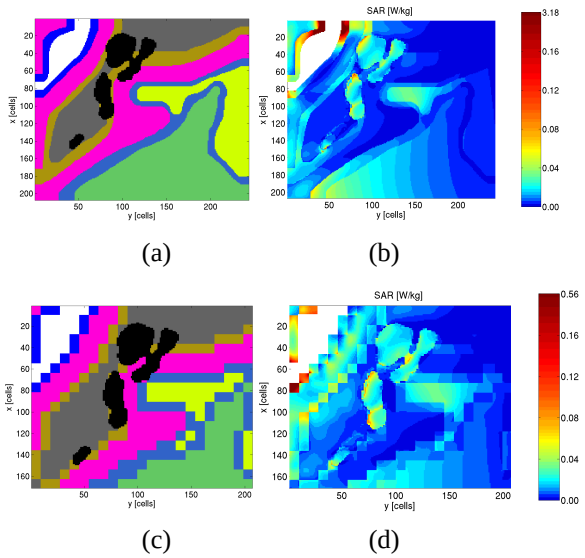

Figure 10: Improvement of the geometrical resolution of the head model in the inner ear region. (a) Smoothed region of the inner ear in the head model. (b) SAR distribution in the smoothed inner ear region. (c) Inner ear region of the original head model. (d) SAR distribution in the original inner ear region.

ISSN: 1727-1983

Discussion

The aim of the study was a detailed computation of the SAR in the region of the inner ear. A detailed inner ear model was inserted into the head model. In the previous paper [9] we reported considerable change of the SAR in the region of the inner ear after insertion of the inner ear model. In this paper we investigated how detailed models need to be used to give reliable results.

The inner ear model used represents the volume of the fluids inside the inner ear, the perilymph and the endolymph. The dielectric properties of the fluids are not known. However, because of the perilymph is similar to spinal fluid, the inner ear model was modelled using the cerebral spinal fluid, which dielectric properties are included in the data set provided by Brooks [4].

The subgridding technique used does not cause difficulties with the stability of the FDTD method, because the subgrid is not coupled back to the parent grid, i.e the subgrid #2 is not coupled back to the subgrid #1 and the subgrid #1 is not coupled back to the main grid. Instead of that, the coupling is achieved in such a manner, that the geometry in the subgrid is transfered to the parent grid with coarser geometrical resolution. Then the time step of the FDTD method can be set to the stability condition criteria provided that the geometry in a region near the boundaries of the subgrid is identically same with the geometry of the parent grid. We keep the thickness of this region equal to one main grid cell size, i.e. 1 mm.

Conclusions

Inclusion of a detailed inner ear model makes a considerable difference in the obtained SAR values. Moreover to get most correct results, both, the geometry of the inner ear and the geometry of the inner ear region in the head model must be improved together.

The volume averaged SAR in the inner ear and the internal acoustic canal is very low, around 30 and 20 mW/kg, respectively. Therefore it is high probable that only non thermal effects are involved for the risk of acoustic neuroma.

In the future we intend to model the vestibulo-cochlear nerve, which pass through the internal acoustic canal, from the inner ear to the brain system. If the vestibulo-cochlear nerve was modelled, the volume averaged SAR in the internal acoustic canal is likely to be even lower, because the properties of the nerve compared to those of the cerebral spinal fluid have lower values.

References

[1] LÖNN, S., AHLBOM, A., HALL, P. AND FEYCHTING, M. Mobile Phone Use and the Risk of Acoustic Neuroma, Epidemiology, Vol. 15, No. 6, 2004.

[2] TAFLOVE, A. Computational Electrodynamics, The Finite-Difference Time-Domain Method, 1995, Artech House, Inc.

[3] ACKERMAN, M. J. The Visible Human Project, *Journal of Biocommun*, 18(2):14.

[4] MASON, P. A., ZIRIAX, J. M., HURT W.D., WALTERS, T. J., RYAN, K. L., NELSON, D. A., SMITH, K. I. AND D'ANDREA, J. A. Recent advancements in dosimetry measurements and modeling, in Radio Frequency Radiation Dosimetry, Klauenberg, B. J. and Miklavcic, D., Eds. Norwell, MA: Kluwer, 2000, pp. 141-155.

[5] GABRIEL, C. Compilation of the dielectric properties of body tissues at RF and microwave frequencies, Report AL/OE-TR-1996-0037, Armstrong Laboratory (AFMC), Radiofrequency Radiation Division, Brooks, AFB, TX.

[6] YEE, K. S. Numerical Solution of Initial Boundary Value Problems Involving Maxwell's Equations in Isotropic Media, *IEEE Transactions on Antennas and Propagation*, AP-14, 1966, pp. 302-307.

[7] CHEVALIER, M. W., LUEBBERS, R. J. AND VAUGHN, P. C. FDTD local grid with material traverse, *IEEE Transactions on Antennas and Propagation*, vol. 45, No.3, March 1997, pp. 411-421.

[8] INTERNATIONAL COMMISSION ON NON-IONIZING RADIATION PROTECTION Guidelines for limiting exposure to time-varying electric, magnetic, and electromagnetic fields (up to 300GHz), 1998, *Health Phys.*, 74, pp. 494-522.

[9] KOPECKÝ, R., PERSSON, M. Modelling of mobile phone exposure to the human head. *EMB 04, Conference Proceedings*, 2004. pp. 276-283.

ISSN: 1727-1983